Journal of Southeast University (English Edition) Vol. 23, No. 1, pp. 105 – 111 Mar. 2007 ISSN 1003—7985

Behavior of interfacial stresses between RC beams and GFRP sheets

Wang Wenwei[1] Li Guo[2]

([1]School of Transportation, Southeast University, Nanjing 210096, China)

([2]Chengxian College, Southeast University, Nanjing 210096, China)

Abstract: Seven reinforced concrete (RC) beams with epoxy-bonded glass fiber reinforced plastic (GFRP) sheets and two control RC beams were experimentally tested to investigate the bond behavior of the interfaces between RC beams and GFRP sheets. The variable parameters considered in test beams are the layers of GFRP sheets, the bond lengths and the reinforcement ratios. The results indicate that the flexural strength of the repaired beams is increased, but the ultimate load of beams with GFRP sheets debonding failure is reduced relatively. The bond length is the main factor that results in bonding failure of the strengthened beams. An experimental method of interfacial shear stress is proposed to analyze the distribution of shear stress according to experimental results. The analytical method of shear and normal stresses and a simple equation are proposed to predict the peeling loads. The proposed model is applied to experimental beams. The analytical results show a good agreement with the experimental results.

Key words: glass fiber reinforced plastic (GFRP); strengthening; reinforced concrete beam; shear stress; normal stress

In recent years, repair and retrofit of existing structures have been among the most important challenges in China. Different techniques have been developed to retrofit the concrete structures. For RC beams, a common repair and retrofit technique is to bond fiber reinforced plastic (FRP) sheets/plates to the bottom of RC beams. Comprehensive experimental investigations conducted in past years have shown that this strengthening method has several advantages, such as lighter weight, higher strength, no corrosion, and easy application procedures at the construction site[1–3].

Previous laboratory studies have demonstrated the effectiveness of externally bonded FRP sheets in enhancing both the flexural capacity and shear capacity of concrete beams in China[4–5]. However, RC beams strengthened with FRP sheets may exhibit FRP sheets debonding failure at the ends of FRP sheets due to high interfacial stresses. This failure, which is usually named shear-tension failure[6], results from a combination of shear and normal stresses in the concrete in the plane of longitudinal steel bars. This failure mechanism can initiate at the end of an FRP sheet, resulting in the propagation of horizontal cracking, and can cause separation of the concrete cover. This paper describes the experimental results and the analytical study concerning the shear-tension failure.

Received 2006-07-21.

Biography: Wang Wenwei (1971—), male, doctor, associate professor, wenwei_wang@163.com.

1 Experimental Program

A total of 9 beams were tested. All beams have identical rectangular cross-sections and the same size: 150 mm × 250 mm × 2 700 mm (see Fig. 1). There are two types of shear span length (1 000 mm and 800 mm) to provide two regions of constant moment: 400 mm and 800 mm. Two beams were used as control specimens and the others were strengthened in flexure using one and two layers of externally bonded GFRP sheets, respectively. Different GFRP lengths with different bond lengths were applied in different beams, respectively (see Tab. 1). Two grades of cube compressive strength of concrete, which are named C20 and C30, were used. The flexural tension reinforcement consisting of 12 mm and 14 mm deformed bars were used. Shear reinforcement consisted of 6 mm-diameter round steel stirrups spaced at 100 mm center-center (see Fig. 1). The GFRP material consisted of 150 mm wide and 0.7 mm thick glass sheets externally bonded to the tension face of the concrete beams using a two-part epoxy mixed at a 2.5∶1 ratio and cured at room temperature. A summary of all the material properties is given in Tab. 2.

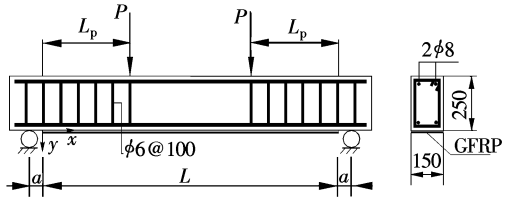

Fig. 1 Details of test beams

Tab. 1 Test specimens and test results

Beam designation	Grade of concrete compressive strength	GFRP	Length of GFRP/mm	a/mm	Bond length L_p/mm	Flexural tension reinforcement ratio ρ_s/%	Load/kN		Failure mode
							At yield	At ultimate	
CL20	C20					0.70(2ϕ12)	30	37	Concrete crushing
CL30	C30					1.43(3ϕ14)	85	102	Concrete crushing
BL20-1	C20	1 layer	2 300	50	950	0.70(2ϕ12)	35	57	GFRP rupture
BL20-2	C20	2 layers	2 300	50	750	1.43(3ϕ14)	100	120	Concrete crushing
BL30-1	C30	1 layer	2 100	150	850	0.70(2ϕ12)	35	58	GFRP rupture
BL40-1	C40	1 layer	1900	250	750	0.70(2ϕ12)	40	60	GFRP rupture
PPL20	C20	1 layer	400	1 000	0	0.70(2ϕ12)	33	45	GFRP debonding
PPL30	C30	1 layer	600	900	100	0.70(2ϕ12)	30	46	GFRP debonding
PPL40	C40	1 layer	800	800	200	0.70(2ϕ12)	34	46	GFRP debonding

Tab. 2 Material properties

Material		f_y/MPa	ε_y/%	f_u/MPa	ε_u/%	E/GPa	G/MPa
Steel	8 mm bar	352.1	1.68	523.9		210	
	12 mm bar	381.7	1.91	579.1		200	
	14 mm bar	365.9	1.83	535.9		200	
Concrete	C20			32.6		30.7	
	C30			40.3		32.7	
GFRP				542	2.46	22	
Resin				52.5		32.4	10.6

A total of three linear voltage displacement transducers (LVDTs) were used to measure midspan, and supporting point deflections. All specimens were tested in four-point bending over a 2.4 m simple span in a 5 000 kN test frame. All beams were statically tested to failure at a load rate of approximately 12 N/s.

2 Test Results and Discussion

2.1 Failure modes

The beams strengthened with GFRP sheets, as shown in Fig. 2 and Tab. 1, exhibited three basic failure modes. The load-midspan displacements of test beams are shown in Fig. 3. The test results are summarized in Tab. 1.

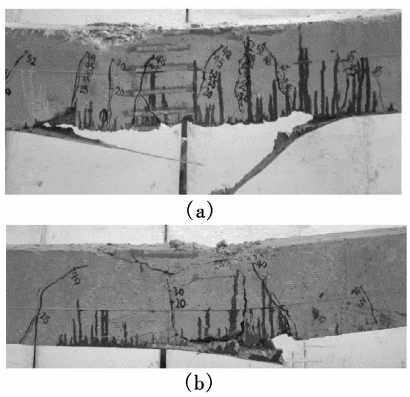

Fig. 2 Failure modes. (a) Rupture of GFRP sheet; (b) Debonding of concrete cover at the end of GFRP

For beams BL20-1, BL30-1, and BL40-1, one layer of GFRP sheet was externally bonded to the tension face of the test beams. The crack load was about 26% to 30% of the ultimate load of the control beam

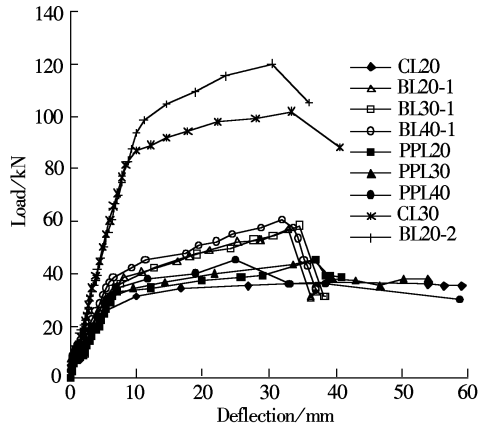

Fig. 3 Load-displacement curves for all test beams

CL20. As the additional loads were applied, flexural cracks were initiated from the bottom of the beams in the region of maximum moment. The main steels yielded at loads of 35 or 40 kN and the old cracks were widened and extended upward and new cracks were initiated. As the applied load was further increased, cracks propagated toward the upper areas of the beams and failure of tensile of GFRP sheets occurred, as shown in Fig. 2(a).

Beam BL20-2, with moderate flexural tension reinforcement ratios, was externally bonded to the tension face of the test beam by two layers of GFRP sheets. Failure occurred by the crushing of the concrete in the compression zone.

For beams PPL20, PPL30, and PPL40, one layer of GFRP sheet was also externally bonded to the tension face of the test beams. The bond length was 0, 100 and 200 mm, respectively. After strengthening, as

the additional load was applied, flexural cracks were initiated from the bottom of the beams in the region of maximum moment. As the applied load was further increased, vertical cracks were initiated at the end of the GFRP sheets and main cracks were formed quickly. The concrete covers at the end of the GFRP sheets started to peel due to the stress concentration and propagated from there to the mid-span of the beams. As the applied load was further increased, the main cracks widened and extended upward continuously and failure of crushing of concrete in the compression zone occurred, as shown in Fig. 2(b). It is shown that the bond lengths of sheet have a direct effect on the debonding failure. It is proposed that bond length should be enough for the strengthening beam externally bonded with GFRP sheets to avoid debonding failure.

2.2 Measuring the interfacial shear stress distribution

To measure the interfacial shear stress distribution at the end of the GFRP sheet, the GFRP sheet was instrumented with five electrical strain gauges distributed along the end of the GFRP sheet, as shown in Tab. 3. Using strain reading from the GFRP sheet, the shear stress distribution can be obtained by curve fitting the strain versus distance-from-cut-off-point and relating the shear stress to the rate of change of strain according to the following equation:

$$\tau(x) = t_p E_p \frac{d\varepsilon(x)}{dx} \quad (1)$$

where E_p is the elastic modulus of GFRP sheet, t_p is the thickness of the GRRP sheet, and $\varepsilon(x)$ is the GFRP sheet strain.

Tab. 3 Location of strain gauges on the end of GFRP sheet

Gauge number	1	2	3	4	5
Distance from beam support/mm	10	20	50	100	150

The shear stress $\tau(x)$ can be also obtained from the following equation[7-8]:

$$\tau(x) = C_1 e^{-cx} + C_2 e^{cx} + D_1 x + D_2 \quad (2)$$

where C_1, C_2, D_1 and D_2 are constants; x is the longitudinal distance from the cut-off-point.

Integrating Eq. (2), we obtain

$$\varepsilon(x) = -Be^{-cx} + Ee^{cx} + \frac{D_1^2}{2}x + D_2 x + D_5 \quad (3)$$

where $B = C_1/(t_p E_p C)$ and $E = C_2/(t_p E_p C)$.

At the end of the GFRP sheet, Eq. (3) can be expressed as

$$\varepsilon(x) = A - Be^{-cx} \quad (4)$$

where $A = E + D_5$.

Substituting Eq. (4) into Eq. (1), Eq. (1) can be expressed as

$$\tau(x) = t_p E_p BC e^{-cx} \quad (5)$$

and the maximum shear stress at the end of the GFRP sheet is calculated as

$$\tau_{max} = t_p E_p BC \quad (6)$$

The constants A, B, C can be obtained by regressing Eq. (4) according to the GFRP strain and the maximum shear stress at the end of the GFRP sheet can be calculated according to Eq. (6). The maximum shear stresses of all test beams were calculated under 40 kN load by Eq. (4) to Eq. (6).

For beam BL30-1, the strain at the end of the GFRP sheet was reading from the acquisition system and we can obtain the regression equation of GFRP strain:

$$\varepsilon(x) = 0.000\,5 - 0.000\,53\exp\left(-\frac{x}{70.160\,52}\right) \quad (7)$$

where $A = 0.000\,5$, $B = 0.000\,53$, $C = 0.014\,25$.

Fig. 4 illustrates the strain distribution at the end of the GFRP sheet and the regression curve of the GFRP strain for beam BL30-1.

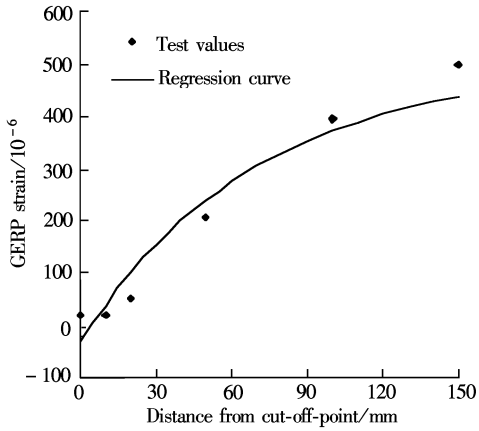

Fig. 4 Strain distribution at the end of GFRP sheet and regression curve for beam BL30-1

3 Analytical Models

In this section, analytical models are developed for predicting the shear and normal stresses at the concrete/FRP interface. Some assumptions made to simplify the problem are as follows: ① Plane cross sections remain plane during loadings; ② FRP, concrete and steel are all linear elastic and of isotropic behavior; ③ There is no slip between FRP and RC beams.

3.1 Shear stress

A RC beam strengthened with an FRP sheet has a rectangular cross-section $b \times h$. The thickness of the FRP sheet and the epoxy layer is t_p and t_a, respectively, as shown in Fig. 5. The shear stress can be defined by considering the equilibrium of an infinitesimal part of the FRP sheet:

$$\tau(x) = t_p \frac{d\sigma_p(x)}{dx} \tag{8}$$

where $\sigma_p(x)$ is the tensile stress in FRP sheet.

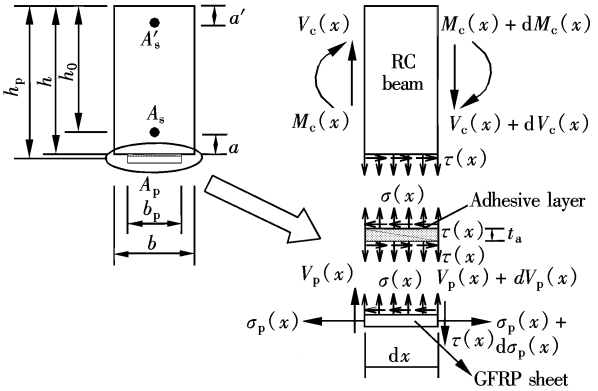

Fig. 5 Cross section and isolated elements

Differentiating Eq. (8) with respect to x, results in

$$\frac{d\tau(x)}{dx} = t_p \frac{d^2\sigma_p(x)}{dx^2} \tag{9}$$

The relationship of shear stress and shear strain γ in the epoxy layer can be written as

$$\tau(x) = \frac{G_a}{t_a}\gamma = \frac{G_a}{t_a}u(x, y) \tag{10}$$

in which

$$u(x, y) = u_2(x) - u_1(x) \tag{11}$$

where G_a is the shear modulus of elasticity of the adhesive layer, $u_1(x)$ is the horizontal displacement of the bottom fiber of RC beam, and $u_2(x)$ is the horizontal displacement of the FRP sheet.

Substituting Eq. (11) into Eq. (10), Eq. (10) can be expressed as

$$\tau(x) = \frac{G_a}{t_a}[u_2(x) - u_1(x)] \tag{12}$$

Differentiating Eq. (12) with respect to x, results in

$$\frac{d\tau(x)}{dx} = \frac{G_a}{t_a}\left[\frac{du_2(x)}{dx} - \frac{du_1(x)}{dx}\right] = \frac{G_a}{t_a}[\varepsilon_2(x) - \varepsilon_1(x)] \tag{13}$$

where $\varepsilon_1(x)$ is the tensile strain of the top fiber of the adhesive layer, and $\varepsilon_2(x)$ is the tensile strain of the bottom fiber of the adhesive layer.

The tensile strain of the bottom fiber of the adhesive layer $\varepsilon_2(x)$ can be written as

$$\varepsilon_2(x) = \frac{\sigma_p(x)}{E_p} \tag{14}$$

Actually, the tensile strain of the top fiber of the adhesive layer $\varepsilon_1(x)$ is the tensile strain of the bottom fiber of the RC beam. For RC beams, the beams are made of two different materials, and one of them, the concrete, does not have a linear stress-strain relationship. Besides, the member under service load is usually cracked transversely and diagonally. So the calculation of tensile strain at the bottom face of the RC beams is cumbersome. The calculation of tensile strain at the bottom face of the RC beams presented in this paper is a simple method.

For a strengthened beam, the depth of neutral axis x_0 can be calculated as

$$\frac{1}{2}bx_0^2 + (\alpha_E A_s + \alpha'_E A'_s + \alpha_{Ef} A_p)x_0 - \alpha_E A_s h_0 - \alpha_E A'_s a' - \alpha_{Ef} A_p h_p = 0 \tag{15}$$

where $\alpha_E = E_s/E_c$ and $\alpha_{Ef} = E_p/E_c$; E_s is the elastic modulus of steel bar; E_c is the elastic modulus of concrete. The moment of inertia of a strengthened beam can be expressed as

$$I_0 = \frac{1}{3}bx_0^3 + \alpha_E A_s(h_0 - x_0)^2 + (\alpha_E - 1)A'_s(x_0 - a')^2 + \alpha_{Ef} A_p(h_p - x_0)^2 \tag{16}$$

The tensile strain of the top fiber of the adhesive layer $\varepsilon_1(x)$ can be written as

$$\varepsilon_1(x) = \frac{M(x)(h - x_0)}{E_c I_0} \tag{17}$$

where $M(x)$ is the bending moment.

Substituting Eq. (14) and Eq. (17) into Eq. (13), Eq. (13) can be expressed as

$$\frac{d\tau(x)}{dx} = \frac{G_a}{t_a}\left[\frac{\sigma_p(x)}{E_p} - \frac{M(x)(h - x_0)}{E_c I_0}\right] \tag{18}$$

Substituting Eq. (18) into Eq. (9), the governing differential equation for tensile stress in the FRP sheet can be expressed as

$$\frac{d^2\sigma_p(x)}{dx^2} - \frac{G_a}{t_a t_p E_p}\sigma_p(x) + \frac{M(x)G_a(h - x_0)}{t_a t_p E_c I_0} = 0 \tag{19}$$

The solution of Eq. (19) is given by

$$\sigma_p(x) = C_3 e^{\alpha x} + C_4 e^{-\alpha x} + \frac{m_1}{\alpha^2}M(x) \tag{20}$$

where $\alpha = \sqrt{\dfrac{G_a}{t_a t_p E_p}}$ and $m_1 = \dfrac{G_a(h - x_0)}{t_a t_p E_c I_0}$; C_3 and C_4 are constants.

Substituting Eq. (20) into Eq. (8), the shear stress can be expressed as

$$\tau(x) = D_3 e^{\alpha x} + D_4 e^{-\alpha x} + t_p \frac{m_1}{\alpha^2}V(x) \tag{21}$$

where $D_3 = \alpha t_p C_3$ and $D_4 = -\alpha t_p C_4$.

The maximum shear stress at the end of FRP can be expressed as

$$\tau_{max} = D_3 + D_4 + t_p \frac{m_1}{\alpha^2}V(0) \tag{22}$$

where $V(0)$ is the shear force at $x = 0$. The constants D_3 and D_4 in Eq. (22) can be obtained according to the different boundary conditions, as shown in Tab. 4. It is shown from Tab. 4 that the expression of the maximum shear stress can be written uniformly as

Tab. 4 Solution of stresses at the end of FRP

Load case	Boundary condition	Solution of stresses at the end of FRP	Maximum stress
Uniformly distributed load	$\sigma_p(0)=0$ $\tau\left(\frac{L}{2}-a\right)=0$ $V\left(\frac{L}{2}-a\right)=0$ $M_p(x)=0$ $V_p(x)=V_p(0)$	$\tau(x)=t_p\frac{m_1}{\alpha}M(0)\,e^{-\alpha x}+t_p\frac{m_1}{\alpha^2}V(x)$ $\sigma(x)=\frac{E_a}{2\beta^3 t_a}\left[\left(\frac{V_p(x)}{E_pI_p}-\frac{V_c(x)+\beta M(x)}{E_cI_c}\right)\cos\beta x+\frac{\beta M(x)}{E_cI_c}\sin\beta x\right]+\frac{q(x)E_pI_p}{b_pE_cI_c}$	$\tau_{max}=t_p\frac{m_1}{\alpha}M(0)+t_p\frac{m_1}{\alpha^2}V(0)$ $\sigma_{max}=\frac{E_a}{2\beta^3 t_a}\left(\frac{V_p(0)}{E_pI_p}-\frac{V_c(0)+\beta M(0)}{E_cI_c}\right)+\frac{q(x)E_pI_p}{b_pE_cI_c}$
Two point loads	$\sigma_p(0)=0$ $\tau\left(\frac{L}{2}-a\right)=0$ $\sigma_p^-(L_0-a)=\sigma_p^+(L_0-a)$ $\tau_p^-(L_0-a)=\tau_p^+(L_0-a)$ $M_p(x)=0$ $V_p(x)=V_p(0)$	$\tau(x)=\begin{cases}\frac{t_pm_1M(0)}{\alpha}e^{-\alpha x}+t_p\frac{m_1}{\alpha^2}V(x) & 0\leqslant x\leqslant L_0-a\\ t_p\frac{m_1}{\alpha}M(0)\,e^{-\alpha x}+t_p\frac{m_1}{2\alpha^2}V(0)\,e^{\alpha(L_0-a)}e^{-\alpha x} & L_0-a\leqslant x\leqslant\frac{L}{2}-a\end{cases}$ $\sigma(x)=\frac{E_a}{2\beta^3 t_a}\left[\left(\frac{V_p(x)}{E_pI_p}-\frac{V_c(x)+M(x)}{E_cI_c}\right)\cos\beta x+\frac{\beta M(x)}{E_cI_c}\sin\beta x\right]$	$\tau_{max}=t_p\frac{m_1}{\alpha}M(0)+t_p\frac{m_1}{\alpha^2}V(0)$ $\sigma_{max}=\frac{E_a}{2\beta^3 t_a}\left(\frac{V_p(0)}{E_pI_p}-\frac{V_c(0)+\beta M(0)}{E_cI_c}\right)$

$$\tau_{max}=t_p\frac{m_1}{\alpha}M(0)+t_p\frac{m_1}{\alpha^2}V(0)=\frac{G_a}{\alpha t_aE_c}\sigma_0+\frac{G_a}{\alpha^2 t_at_pE_c}\tau_0 \tag{23}$$

where $M(0)$ is the bending moment at $x=0$, $\sigma_0=\frac{M(0)(h-x_0)}{I_0}$ and $\tau_0=\frac{t_pb_p(h-x_0)}{b_pI_0}V(0)$.

3.2 Normal stress

In Fig. 5, the fourth-order differential equation for the strengthened beam can be expressed as[7]

$$\left.\begin{aligned}-E_cI_c\frac{d^4v_1}{dx^4}&=q(x)-b_p\sigma(x)\\ -E_pI_p\frac{d^4v_2}{dx^4}&=b_p\sigma(x)\end{aligned}\right\} \tag{24}$$

where $\sigma(x)$ is the normal stress; v_1 and v_2 are the vertical deflections of the FRP sheet and concrete beam, respectively.

$$I_c=\frac{1}{3}bx_c^3+\alpha_EA_s(h_0-x_c)^2+(\alpha_E-1)A_s'(x_c-a')^2 \tag{25}$$

$$I_p=\frac{1}{12}b_pt_p^3 \tag{26}$$

where x_c is the depth of the neutral axis of the RC beam, I_c is the moment of inertia of the RC beam, and I_p is the moment of inertia of the FRP sheet.

For an RC beam, the depth of neutral axis x_c can be calculated as

$$\frac{1}{2}bx_c^2+(\alpha_EA_s+\alpha_E'A_s')x_c-\alpha_EA_sh_0-\alpha_EA_s'a'=0 \tag{27}$$

The normal stress $\sigma(x)$ can also be written as

$$\sigma(x)=\frac{E_a}{t_a}(v_2-v_1) \tag{28}$$

Differentiating Eq. (28) four times and solving Eq. (24) for $\frac{d^4v_1}{dx^4}$ and $\frac{d^4v_2}{dx^4}$ and substituting the corresponding values in Eq. (28) gives the governing differential equation of normal stress:

$$\frac{d^4\sigma(x)}{dx^4}+\frac{E_ab_p}{t_aE_pI_p}\sigma(x)=\frac{E_a}{t_aE_cI_c}q(x) \tag{29}$$

The solution of this fourth-order linear differential equation is given below:

$$\sigma(x)=e^{-\beta x}(E_1\cos\beta x+E_2\sin\beta x)+e^{\beta x}(E_3\sin\beta x+E_4\cos\beta x)+\frac{q(x)E_pI_p}{b_pE_cI_c} \tag{30}$$

where $\beta=\left(\frac{E_ab_p}{4t_aE_pI_p}\right)^{\frac{1}{4}}$; E_1 to E_4 are the constants of integration; and $q(x)$ is the uniformly distributed load. The constants E_1 to E_4 in Eq. (30) can be obtained according to different boundary conditions, as shown in Tab. 4. The shear force $V_p(x)$ at a small element shown in Fig. 5 is determined by

$$V_p(x)=b_pt_p\tau(x) \tag{31a}$$

and $V_p(0)$, as shown in Tab. 4, can be written as

$$V_p(0)=b_pt_p\tau_{max} \tag{31b}$$

The terms $V_c(0)+\beta M(0)$ and E_pI_p are relatively small compared to E_cI_c and have been neglected in the solution of normal stress, as shown in Tab. 4. So the normal stress can be expressed as

$$\sigma_{max}=\frac{b_pt_pE_a}{2\beta^3t_aE_pI_p}\tau_{max}=\psi\tau_{max} \tag{32}$$

where $\psi=\frac{b_pt_pE_a}{2\beta^3t_aE_pI_p}$.

3.3 Peeling load

The principle stresses using the stress transformation are as follows[8]:

$$\sigma_{1,2}=\frac{\sigma_{max}}{2}\pm\sqrt{\left(\frac{\sigma_{max}}{2}\right)^2+\tau_{max}^2}=\frac{\tau_{max}}{2}(\psi\pm\sqrt{\psi^2+4}) \tag{33}$$

where σ_1 and σ_2 are principle stresses.

For the tension-compression state of stress, fail-

ure criterion of concrete is given by[9]

$$\sigma_1 = \left(1 - 0.8\frac{\sigma_2}{f_c}\right) f_t \tag{34}$$

Realizing that the ratio of σ_2/f_c is very small, an approximation of Eq. (34) is given by

$$\sigma_1 = 0.95 f_t \tag{35}$$

Substituting Eq. (33) into Eq. (35), Eq. (35) can be expressed as

$$\sigma_1 = \frac{\tau_{max}}{2}(\psi + \sqrt{\psi^2 + 4}) = 0.95 f_t \tag{36}$$

Substituting Eq. (23) into Eq. (36), Eq. (36) can be expressed as

$$P_{peel} = \frac{1.9\alpha^2 f_t}{t_p m_1 (\alpha a + 1)(\psi + \sqrt{\psi^2 + 4})} \tag{37}$$

where P_{peel} is the peeling load, and a is the distance between the support point and the cut-off point of the FRP sheet.

To ascertain the accuracy of the proposed method, Eqs. (23), (32) and (37) were used to predict the maximum shear and normal stresses and peeling loads for GFRP-strengthened beams were tested in four-point bending under a 40 kN load and compared with Roberts' expression[10], as shown in Tab. 5.

Tab. 5 Calculation values of stress and peel load at the end of FRP

Beam designation	Load = 40 kN					Peeling load/kN	
	Maximum shear stress/MPa			Maximum normal stress/MPa			
	Regression value	Roberts' expression	Calculation value	Roberts' expression	Calculation value	Experimental value	Calculation value
BL20-1	0.012	0.113	0.087	0.091	0.129		540.44
BL20-2	0.020	0.104	0.075	0.092	0.129		567.76
BL30-1	0.166	0.276	0.186	0.206	0.275		292.27
BL40-1	0.184	0.441	0.283	0.329	0.417		218.45
PPL20	0.819	1.326	1.028	0.703	1.512	45	39.05
PPL30	0.833	1.271	0.925	0.672	1.361	46	43.42
PPL40	0.742	0.943	0.823	0.634	1.212	46	48.77

4 Conclusions

1) GFRP external reinforcement obviously increased beam ultimate flexural capacities, but the ultimate load of beams with GFRP sheets debonding failure was relatively reduced.

2) The experimental method was proposed to analyze the shear distribution at the end of the FRP sheet according to reading tested values of FRP strain.

3) The peeling load gradually increased along with increasing bond length and concrete strength and decreasing thickness of the FRP sheet.

4) A simple approach was presented to predict the maximum shear and normal stresses and peeling load for strengthened beams. Excellent correlation of the predicted results with experimental results was noted.

References

[1] Wang Wenwei, Zhao Guofan, Huang Chengkui, et al. Experimental study of strengthening of reinforced concrete beams with externally bonded GFRP sheets [J]. *Journal of Dalian University of Technology*, 2003, **43**(6): 799 − 805. (in Chinese)

[2] Wang Wenwei, Li Guo. Experimental study and analysis of RC beams strengthened with CFRP laminates under sustaining load [J]. *International Journal of Solids and Structures*, 2006, **43**(3): 1372 − 1387.

[3] Yao W. Flexural strength and behavior of polypropylene fiber reinforced concrete beams [J]. *Journal of Wuhan University of Technology*: *Materials Science Edition*, 2002, **17**(3): 54 − 57.

[4] Wang Wenwei, Zhao Guofan, Huang Chengkui, et al. An experimental study of strengthening of initially loaded reinforced concrete beams using CFRP sheets [J]. *Engineering Mechanics*, 2001, **21**(4): 172 − 178. (in Chinese)

[5] Ye Lieping, Zhao Shuhong, Yue Qingrui, et al. Calculation of shear strength of concrete column strengthened with carbon fiber reinforced plastic sheet [J]. *Journal of Building Structures*, 2000, **21**(2): 59 − 67. (in Chinese)

[6] Arduini Marco, Tommaso Angelo Di, Nanni Antonio. Parametric study of beams with externally bonded FRP reinforcement [J]. *ACI Structural Journal*, 1997, **94**(5): 493 − 501.

[7] Malek Amir M, Saadatmanesh Hamid, Ehsani Mohammad R. Prediction of failure load of RC beams strengthened with FRP plate due to stress concentration at the plate end [J]. *ACI Structural Journal*, 1998, **95**(1): 142 − 153.

[8] Xu Zhilun. *Elasticity mechanics* [M]. Beijing: Higher Education Press, 1978. (in Chinese)

[9] Guo Zhenhai. *Theory of reinforce concrete structures* [M]. Beijing: Tsinghua University Press, 1999. (in Chinese)

[10] Roberts T M. Approximate analysis of shear and normal stress concentration in the adhesive layer of plated RC beams [J]. *Structural Engineering*, 1989, **12**: 228 − 233.

GFRP 布与钢筋混凝土梁界面之间应力行为

王文炜[1] 李 果[2]

([1] 东南大学交通学院, 南京 210096)
([2] 东南大学成贤学院, 南京 210096)

摘要:为了解玻璃纤维(GFRP)布与钢筋混凝土梁界面之间的粘结性能,进行了 7 根 GFRP 布加固的钢筋混凝土梁与 2 根对比梁的试验研究. 试验的变化参数为 GFRP 布层数、粘结长度及配筋率. 试验结果表明,GFRP 布加固的钢筋混凝土梁极限荷载显著提高,但是发生剥离破坏的试验梁极限荷载有所降低,粘结长度是影响加固梁剥离破坏的主要因素. 根据试验结果提出了 GFRP 布与钢筋混凝土梁界面粘结剪应力的试验分析方法并分析了界面间粘结剪应力的分布. 同时,提出了 GFRP 布加固的钢筋混凝土梁剥离正应力与粘结剪应力的理论分析方法. 最后,给出了 GFRP 布加固钢筋混凝土梁剥离荷载的计算方法. 为验证理论分析方法的正确性,计算了试验梁界面间的粘结剪应力、剥离正应力及剥离荷载. 计算结果表明,所提出的理论分析方法与试验值吻合较好.

关键词:GFRP 布;加固;钢筋混凝土梁;剪应力;正应力
中图分类号:TU582. 57